# USE OF MODELLING TO CHARACTERIZE THE RISK OF HOT CRACKING IN AUSTENITIC STAINLESS STEELS DURING WELDING

G. TRAN VAN*'**, D. CARRON**, P. LE MASSON**,
J. STODOLNA***, A. ANDRIEU***, J. DELMAS* and V. ROBIN*

*EDF R&D, Chatou, France
**Univ. Bretagne Sud, UMR CNRS 6027, IRDL, F-56100, Lorient, France
***EDF R&D, Renardières, France, vincent.robin@edf.fr

DOI 10.3217/978-3-85125-615-4-27

ABSTRACT

Liquation cracking may occur in the heat affected zone (HAZ) during welding. Two factors influence this phenomenon: the tensile stresses generated during welding and the potential loss of ductility due to the presence of a liquid film at grain boundaries depending on their chemical composition.
Gleeble hot-ductility tests have been used to study the combined effect of boron content and holding time on ductility drop in the liquation temperature range of a 316L type austenitic stainless steel. It is shown that high boron contents and short holding times promote the loss of ductility in the liquation temperature range. Secondary ion mass spectrometry (SIMS) has been used to correlate mechanical results to boron distribution either at grain boundaries or in the bulk.
Other weldability tests have been performed to confirm the influence of boron content on hot cracking sensitivity of AISI 316L stainless steels. Results indicate that cracks appear on all specimens but at different strain levels. The higher boron content is, the more specimen exhibits tendency to hot cracking. Thanks to numerical modelling of these tests, a cracking criteria is proposed to quantify the risk of liquation cracking for different boron contents.

Keywords: Welding, Hot Cracking, Austenitic Stainless Steel, Boron

## INTRODUCTION

Many welded components of pressurized water reactors are made of austenitic stainless steels. During welding of these materials hot cracking due to solidification cracking and/or liquation cracking must be prevented. The influence of harmful elements as sulphur, phosphorus, boron, silicon, niobium and titanium on fully austenitic stainless steel cracking sensitivity is well documented [1][2][3]. With a very low solubility in austenite at high temperature and its tendency to form low melting eutectics with iron and nickel, boron has

a particularly unfavourable influence on hot cracking resistance of austenitic stainless steel [1][3]and nickel-based superalloys [4][5][6][7]. Even at very low contents, boron favours the phenomenon of heat-affected zone (HAZ) liquation cracking which occurs when both intergranular liquid films and sufficient strains are present. In nickel-based superalloys, this intergranular microfissuring phenomenon is associated with constitutional liquation of precipitates at grain boundaries [5][8][9] or grain boundary segregation of melting point depressant elements as boron [4][6][7]. As reported in literature [1], HAZ liquation cracking can also occur during welding of 18Cr-10Ni austenitic stainless steels due to the presence of intergranular austenite / $(FeCr)_2B$ eutectic phase with a low melting point of 1180°C [10][11]. During welding, the temperature in the HAZ can reach the melting temperature of this eutectic phase, which leads to the presence of a liquid phase at the grain boundaries. If the thermal stresses due to welding and self-restraint are sufficiently high, liquation intergranular cracks may appear in the HAZ close to the fusion zone.

To avoid the problem of HAZ liquation cracking, the specification of nuclear fabrication French code RCC-M requires the boron content to be less than or equal to 18 ppm for all of the austenitic stainless steels. However, for the steel of the type 321, the literature shows that there is no cracking if the boron content is less than 35 ppm [10][11]. To rule on the acceptability of these boron-alloyed products, it is essential to better characterize their hot cracking behaviour with respect to the boron content. In this work, Gleeble hot-ductility testing and Varestraint and PVR [12] welding test were achieved to analyse the effect of boron content on hot cracking susceptibility in type 316L austenitic stainless steel. These tests were evaluated to confirm the underlying metallurgical mechanisms. The set of tests also shows that the threshold of 18 ppm is particularly severe for the studied alloy.

Finally, the simulation of the PVR type weldability tests allowed access to the local thermo-mechanical conditions that lead to grain decohesion in a HAZ sensitive to hot cracking. The proposed criteria for estimating the risk of cracking is based on a critical stress and a holding time which are two elements depending on the welding configuration and process. The elevation of the threshold on boron content of austenitic stainless steels can be ensured experimentally by classification of the risk of cracking according to the boron content from weldability tests or by simulation demonstration that the critical conditions in terms of stress and holding times are not reached in a given welding configuration.

## EXPERIMENTAL WORK

Seven AISI type 316L austenitic stainless steels were used in this study. Their chemical composition are shown in Table 1. Three of them, designated by the letters A, B and C, were industrially manufactured and have a boron content of 2±1 ppm, 19±2 ppm and 31±2 ppm respectively. Four of them, designated by the letters D, E, F and G, were experimental alloys with identical composition than alloy C except for the boron content which was 20±2 ppm, 35±3 ppm, 44±4 ppm and 50±4 ppm respectively. Cast ingots of these alloys were prepared by UGITECH (Ugine, France) using vacuum induction melting and hot rolled to 11-mm-thick-plates at 1250°C. Experimental alloys were solution heat treated at 1050°C for 50 minutes and water quenched according to the common industrial process.

Measurements of boron content was realized by inductively coupled plasma mass spectrometry (ICP-MS).

**Table 1** Chemical compositions of the 316L stainless steels (wt % except for boron content in ppm)

| Steel | B (ppm) | C | Mn | Si | P | S | Cr | Ni | Mo | Co | Cu | Al | N |
|---|---|---|---|---|---|---|---|---|---|---|---|---|---|
| **A** | 2±1 | 0.020 | 1.40 | 0.510 | 0.040 | 0.026 | 16.90 | 10.20 | 2.0 | 0.340 | 0.410 | <0.004 | 0.074 |
| **B** | 19±2 | 0.014 | 1.40 | 0.400 | 0.030 | 0.029 | 16.70 | 10.10 | 2.0 | 0.130 | 0.480 | 0.010 | 0.042 |
| **C** | 31±2 | 0.018 | 1.58 | 0.513 | 0.027 | 0.001 | 16.95 | 10.05 | 2.06 | 0.084 | 0.105 | - | 0.048 |
| **D** | 20±2 | 0.019 | 1.56 | 0.540 | 0.031 | 0.0015 | 16.97 | 10.07 | 2.06 | 0.087 | 0.106 | 0.033 | 0.043 |
| **E** | 35±3 | 0.017 | 1.54 | 0.550 | 0.026 | 0.0014 | 16.87 | 10.04 | 2.06 | 0.082 | 0.108 | 0.033 | 0.051 |
| **F** | 44±4 | 0.016 | 1.59 | 0.540 | 0.027 | 0.0011 | 17.25 | 10.03 | 2.05 | 0.080 | 0.106 | 0.043 | 0.052 |
| **G** | 50±4 | 0.016 | 1.61 | 0.540 | 0.027 | 0.0017 | 17.03 | 10.08 | 2.06 | 0.082 | 0.107 | 0.035 | 0.050 |

A Gleeble 3500 thermo-mechanical simulator was used to achieve hot ductility tests in vacuum. Test specimens, of 6 mm in diameter and with a 16 mm free span between water-cooled grips, were heated according to a predetermined thermal cycle and fractured at temperatures between 1150°C and 1350°C by applying a tensile load with a stroke rate of 50 mm/s. After the test, fracture surfaces are examined using a scanning electron microscope JEOL JSM 6460-LV and ductility is determined in terms of the reduction in area by comparing final and initial section area of the broken specimen. On-heating and on-cooling tests were realized. For on-heating tests, the heating rate was 100°C/s and the influence of isothermal holding time before applying the tensile load at testing temperature was studied with holding time varying between 0.1 and 3s. For on-cooling tests, the heating rate was also 100°C/s and two peak temperatures of 1330°C and 1360°C were considered. Once the peak temperature was reached the specimen was subsequently cooled at 80°C/s before to be fractured after a holding time of 0.2s at testing temperature. For alloy F, the influence of the holding time on boron distribution was also characterized by Secondary-Ion Mass Spectrometry (SIMS) analysis. Prior to SIMS analysis, two thermal treatments identical to on-heating hot ductility thermal cycles with 0.1s and 2.5s holding time at 1220°C respectively, but with a cooling rate of the order of 300°C/s, where achieved into a LINSEIS quenching dilatometer (RITA). As received and heat treated F-alloy samples were electrolytically etched in 10% oxalic acid. SIMS analysis was then performed on a CAMECA IMS5F ion microscope using primary ion beam of $O2+$ (15kV acceleration voltage, 1 μA beam current). The negative secondary ions emitted from the surface were $BO2-$. Varestraint and PVR tests were carried out on the materials D, E, F and G with 20 ppm, 35 ppm, 44 ppm and 50 ppm of boron content respectively. The dimensions of the Varestraint specimens were 200 × 60 × 7 mm. The dimensions of PVR specimens were 300 × 40 × 3 mm. The welding parameters of Varestraint and PVR tests, achieved with a single melt run with TIG welding, were kept constant and are shown in Table 2.

**Table 2** TIG welding parameters of the Varestraint and PVR tests

| Parameters of Varestraint tests | | Parameters of PVR tests | |
|---|---|---|---|
| Current | 200A | Current | 81A |
| Voltage | 13V | Voltage | 8.4V |
| Travel speed | 2.33 mm/s | Travel speed | 2.00 mm/s |
| Shielding gas | Argon | Shielding gas | Argon |
| Strain level (47 mm die block radius) | 7% | Maximal stroke rate | 20 mm/min |

A part of the welding surface of F-specimen containing cracks were electrolytically etched using 10% oxalic to reveal the microstructure of grains, and then observed at the binocular.

## EXPERIMENTAL RESULTS

### GLEEBLE HOT-DUCTILITY TESTING AND HAZ LIQUATION CRACKING SUSCEPTIBILITY

On-heating and on-cooling Gleeble tests can be used to evaluate HAZ liquation cracking susceptibility [13][14]. The on-heating test consists of heating the specimen until a predetermined temperature, of holding at this temperature during a certain time and of fracturing the specimen by applying a tensile load with a constant stroke rate. When the testing temperature is raised, ductility may increase slightly then suddenly drop until it reaches almost zero at the nil ductility temperature (NDT). If low-melting point eutectics are present as grain-boundary precipitates or if segregation of impurities to grain boundaries reducing the melting temperature of the boundaries relative to the surrounding matrix has occurred, the increase in temperature leads the grain boundary to melt and the sudden drop in ductility occurs at lower temperature. In this case the ductility drop temperature is representative of the metallurgical degradation associated with grain boundary melting and NDT can then be considered as the temperature where a thin continuous liquid film coats the grain boundary surfaces. As the testing temperature is increased, the nil-strength temperature (NST) is reached where the amount of liquid is high enough that the boundaries are unable to accommodate any stress. On-cooling ductility tests are achieved typically with peak temperature between NDT and NST and the ductility recovery temperature (DRT) is determined when the alloy regains measurable ductility due to a sufficient solidification of the liquid formed during the heating cycle. Various criterion exist to interpret hot ductility tests for assessing HAZ liquation cracking susceptibility, the temperature range NST-DRT being the most widely utilized. Lin et al. [14] having noticed that this criteria may not be representative of HAZ liquation cracking that occurs close to the fusion boundary, had rather suggested a methodology to quantify a thermal-crack susceptible region (CSR) in the HAZ where liquation may occur. On heating and on-cooling CSR can be determined using the temperature range between NDT and the liquidus temperature and the temperature range between on-cooling peak temperature and DRT respectively.

*On-heating hot ductility tests*

As explained previously, the ductility drop with temperature highlighted by on-heating tests is a relevant information to evaluate HAZ liquation cracking susceptibility. In Fig. 1 the results of the on-heating tests achieved with the seven materials with a holding time of 1.0s at the testing temperature are compared. A noticeable difference exists between ductility evolution with temperature for high (F, G) and low and medium boron-level (A to E) alloys. To better highlight this behaviour, the ductility drop temperature was determined as the temperature where ductility decreases to 75% which corresponds to a reduction of one half of the diameter of the specimen. Fig. 2 shows the dependence of this temperature as a function of the boron content. At boron level lower or equal to 35 ppm, ductility drop temperature has an almost constant value around 1320°C. This temperature decreases abruptly if the boron content exceeds this value and then levels out around 1180°C for the alloys with 44 and 50 ppm boron content.

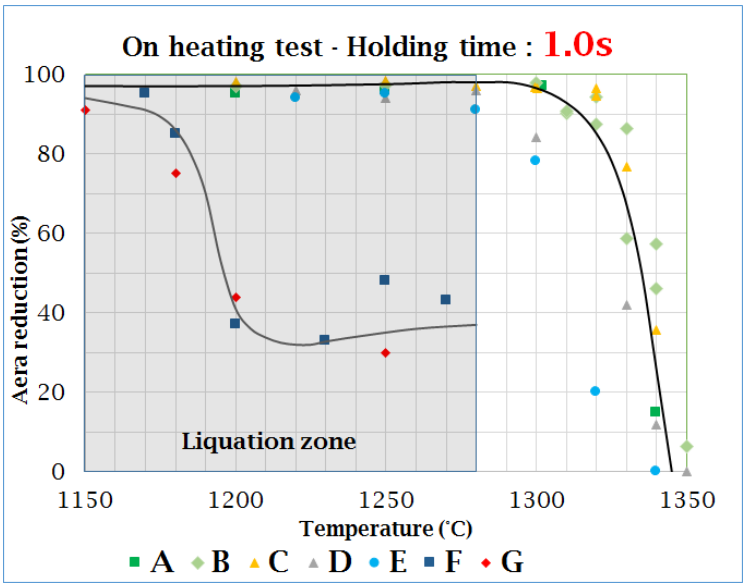


**Fig. 1**: Results of the on-heating tests with a holding time of 1.0s (A=2, B=19, C=31, D=20, E=35, F=44, G=50 ppm of boron respectively)

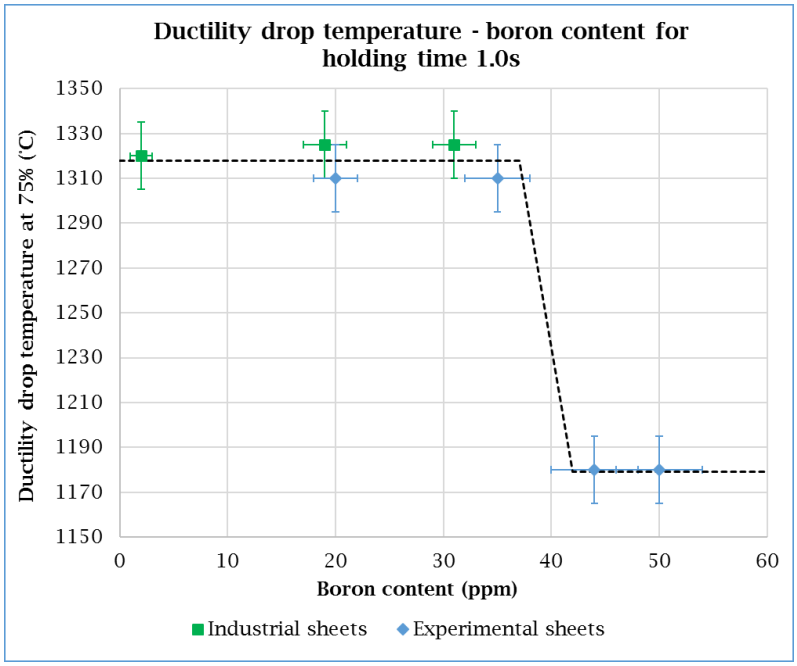


**Fig. 2**:Dependence of the ductility drop temperature with respect to boron content.

It is known that in austenitic stainless steel, because of the low solubility of boron in Fe-Cr-Ni alloys and the formation of boride-austenitic matrix low-melting eutectics at grain boundaries, boron has a detrimental effect on liquation susceptibility and thus lowers the ductility drop temperature even at low content [11][15]. Furthermore, due to non-equilibrium intergranular boron segregation occurring during the heat treatment cooling stage prior to welding, thin boron-enriched zone formation around grain boundary surface can also take place as shown in type 316L stainless steel [16]. As demonstrated for an Inconel alloy [7], it is also suggested a direct correlation between the amount of boron segregated at grain boundaries and the susceptibility to HAZ cracking once again because of the lower melting point of boron-enriched grain boundaries. In very low boron level type 321 and 316 stainless steels that do not experiment liquation cracking phenomena on welding, the ductility drop temperature is over 1300°C. Between 35 and 45 pm of boron this temperature falls suddenly to 1280°C. At higher boron level, when intergranular boride eutectics were clearly identified, this temperature is around 1200°C [11]. The dependence of the ductility drop temperature with respect to boron content for the seven alloys tested in this study is thus consistent with the literature. When the holding time at the testing temperature is 1.0s, grain boundary melting must take place for boron level over 44 ppm with a ductility drop temperature around 1200°C that is close to the austenite-boride eutectic melting temperature. When intergranular boron enrichment is insufficient to promote grain boundary melting, i.e. when boron content is here under 35 ppm, the ductility drop temperature is over 1300°C and it is considered that the material has no risk of HAZ liquation cracking. The transition zone is between 35 and 44 ppm. The temperature range where liquation may occur - i.e. “liquation zone” on Figure 1 - was defined between 1150 and 1280°C.

The literature [10] shows that increasing the holding time at on-heating testing temperature may reduce the risk of ductility drop into the liquation zone for type 321 stainless steels containing high boron content. Compared to welding it is similar to an increase of the magnitude of the heat input [16] since the higher the weld heat input the longer time the HAZ material spent at peak temperature. Therefore to confirm this effect, different welding representative holding times between 0.1 and 3s were considered for tests achieved on materials F (44 ppm) and G (50 ppm) that present the highest risk of HAZ liquation cracking.

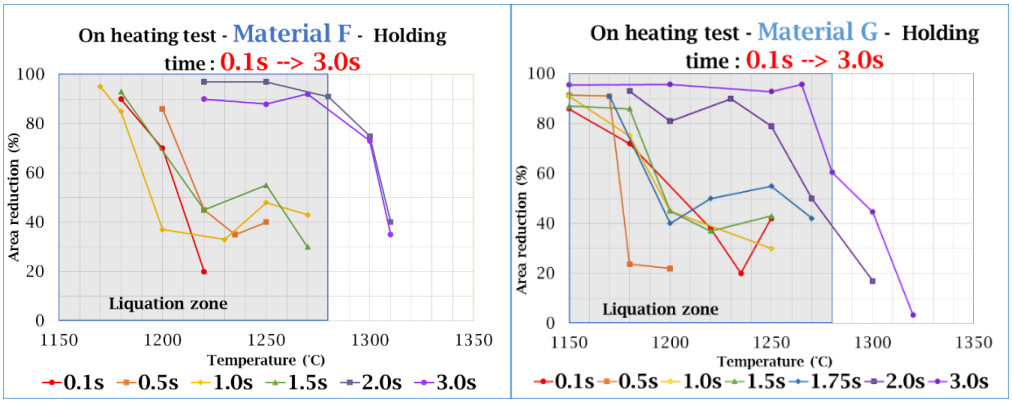


**Fig. 3**:Results of on-heating tests on two materials F (44 ppm B) and G (50 ppm B) with holding time from 0.1s to 3.0s.

It can be seen in Fig. 3 that the ductility drop temperature increases with increase in holding time for all of these two materials. This increase is abrupt with a holding time threshold between 1.5s and 2.0s. The ductility drop temperature for a holding time of 2.0s is actually much higher than that observed with 1.5s. Scanning electron microscopy (SEM) observation of the fracture surface of the F-specimens with 0.1s holding time confirms ductile failure in specimen tested at 1180°C (Fig. 4) and brittle intergranular failure in specimen tested at 1220°C (Fig. 5) that is consistent with a decrease of ductility with the testing temperature from 90% to 20% respectively. For comparison the fractograph of G-specimens tested at 1200°C with 0.5s (brittle failure mode, Fig. 6) and 3s (ductile failure mode, Fig. 7) are consistent with an increase of ductility with holding time from 22% to 96% respectively. Fracture surfaces show features that are consistent with SEM images obtained on 304B grade B boron-containing austenitic stainless steel hot ductility-tested specimens [13]. In particular intergranular mode of fracture is also found at a testing temperature around 1200°C. But one can note no clear evidence of large amount melted liquated film since the amount of boron in our alloys is largely lower than the 1.30 wt% boron content in 304B grade B austenitic stainless steel. Nevertheless small quantities of eutectic liquid coating the grain boundaries could be present given the rather smooth aspect of some grain boundaries appearing in Fig. 5 and Fig. 6.

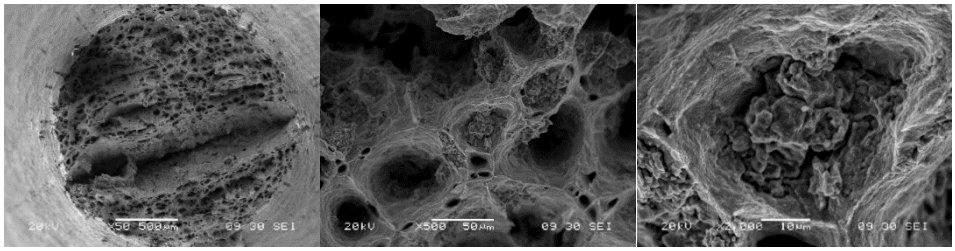

**Fig. 4**: SEM fractograph of Gleeble on-heating F-specimen tested at 1180°C with holding time of 0.1s.

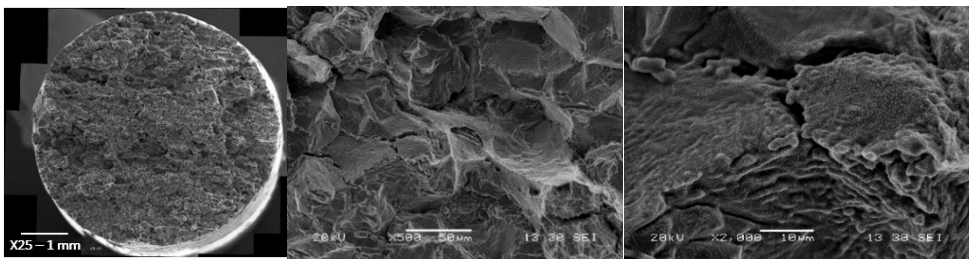


**Fig. 5**: SEM fractograph of Gleeble on-heating F-specimen tested at 1220°C with holding time of 0.1s.

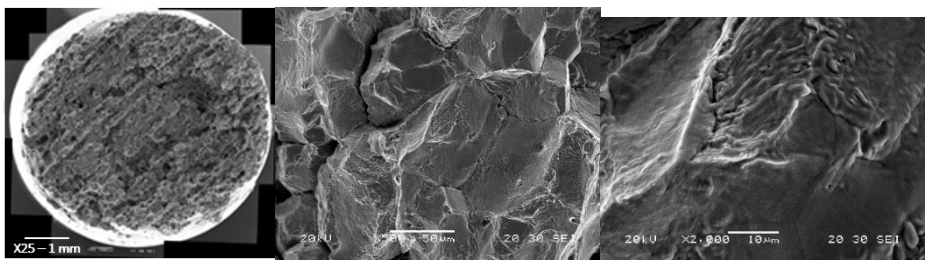


**Fig. 6**: SEM fractograph of Gleeble on-heating G-specimen tested at 1200°C with holding time of 0.5s.

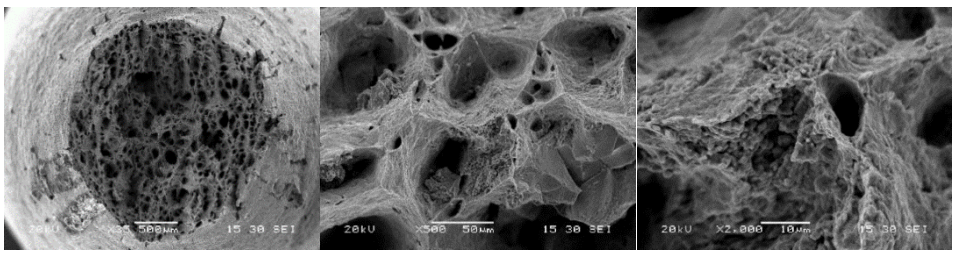

**Fig. 7**: SEM fractograph of Gleeble on-heating G-specimen tested at 1200°C with holding time of 3s.

To better understand the influence of the holding time at microstructural scale, thermal treatments with holding times 0.1s and 2.5s at 1220°C and the same thermal cycles than corresponding hot ductility tests were realised using a quenching dilatometer on material F. After the holding time, these samples were cooled to room temperature at 300°C/s in an attempt to freeze the microscopic structure and their boron distribution was characterized by SIMS analysis. The Figure 8 shows the results of SIMS analysis of the material F in the as received state and after two different heat treatments. Positions of boron appear in light on the pictures.

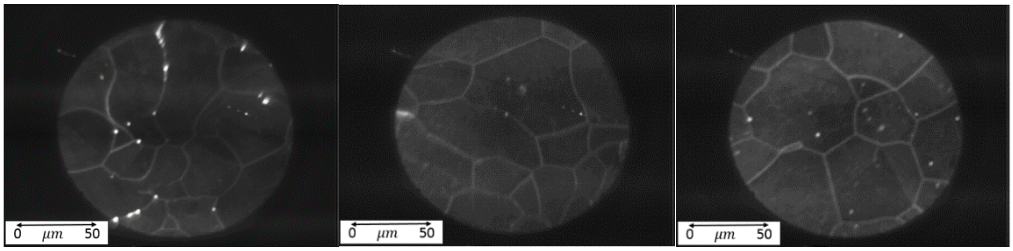


**Fig. 8**: Results of SIMS analysis of the material F: as-received (left), heat treatment at 1220°C with 0.1s of holding time (middle), and heat treatment at 1220°C with 2.5s of holding time (right).

In the as-received material, large intergranular borides that concentrate boron together with some boron segregation at grain boundaries are observed. After heat treatment at 1220°C, the boron concentration decreases but segregation still remains at the grain boundaries with no clear differences between the samples with 0.1 and 2.5s holding time. However, one can note that intragranular precipitates that are nearly absent after a holding time of 0.1s seem more present after a holding time of 2.5s. Since the SIMS analysis is not a quantitative analysis the boron concentration at grain boundaries of these two samples may nevertheless be different. Furthermore, even at a cooling rate of 300°C/s non-equilibrium grain boundary segregation may occur [17]. It is thus difficult to draw a conclusion on the microstructural origin of the increase of ductility drop temperature with holding time. However, it can be hypothesized that there is some boron diffusion from grain boundaries towards the austenitic matrix even during short holding times and that it becomes sufficient to prevent grain boundary melting after a few seconds.

### *On-cooling hot ductility tests*

Influence of boron content and holding time on ductility drop temperature were highlighted by the heating tests. However, liquation cracks appear the most often in HAZ during cooling because the stresses are in tension at this stage of the welding cycle. Gleeble on-cooling tests were thus achieved to complement on-heating tests. It consists of heating the sample to a peak temperature then cooling it to the test temperature and finally rapidly applying a tensile load without holding time to break the sample (Fig. 9). Chosen peak temperatures are Tpeak =1330°C and Tpeak=1360°C. In order to be able to compare with the results of

the on-heating tests, duration time over the testing temperature on heating was added with those on cooling that defined an equivalent holding time (Fig. 9, left). On-heating and on-cooling tests achieved at the same testing temperature and for the same holding /equivalent time were compared in Fig. 9 (right). A coherence between the on-heating and on-cooling results thus appears. During this equivalent time, in agreement with the literature, it is actually considered that boride eutectics stay liquid if temperature is over 1200°C. Thus, neglecting the variation of boron diffusion coefficient with the temperature, the same boron diffusion from grain boundaries towards the austenitic matrix must occur during the holding time for on-heating test or during the high-temperature excursion for on-cooling tests. Indeed, for the low temperature test achieved under 1260°C, the duration time is long and there is no risk of cracking. For the high temperature test, the duration time becomes shorter, ductility falls down and the risk of cracking increases.

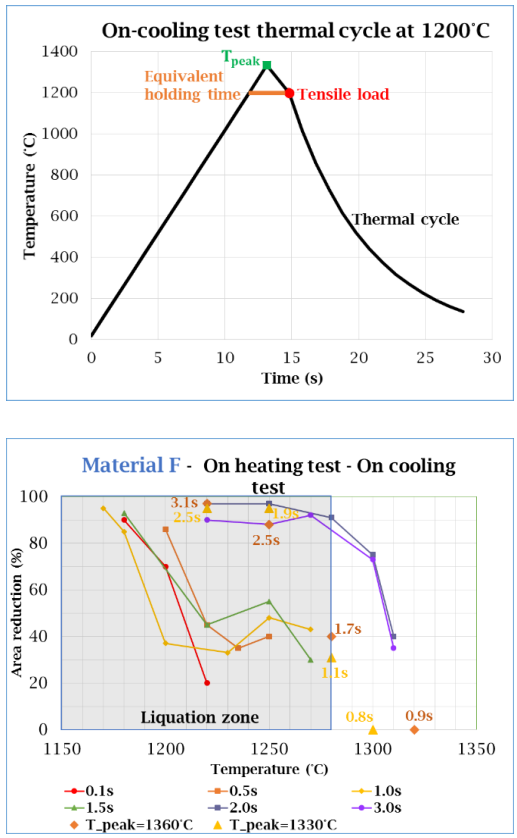


**Fig. 9**: Definition of an equivalent holding time for the on cooling test (left), comparison the results of the on heating test and the on cooling test (right).

WELDABILITY TESTS

Hot ductility testing permits to determine the sensibility of the material to the HAZ liquation cracking but does not take into account the thermal stress induced by welding operation. In order to approach as closely as possible, the real welding conditions Varestraint and PVR tests were achieved.

*Varestraint tests*

Varestraint test consists of making a weld line then of bending quickly the sheet when the welding passes the point of contact between the specimen and the mandrel torch [14][18][19]. Welding continues while the bending is applied. The strain is parallel to the welding direction. The welding surface is then examined. The extent of cracking observed is an indication of the sensitivity to hot-cracking. Fig. 10 shows the macrographs of welded sheets of D, E, F and G materials with 20 ppm, 35 ppm, 44 ppm and 50 ppm of boron content respectively. Most of the cracks appearing in these macrographs are solidification cracks occurring into the fusion zone. A SEM image of one of these solidification cracks in F material is showed in Fig. 11 (left). Few cracks, which are hardly visible on the macrographs, are located near the fusion boundary. Cracking along grain boundaries is visible on SEM images of these latter (Fig. 11, right) which is coherent with liquation cracking phenomenon.

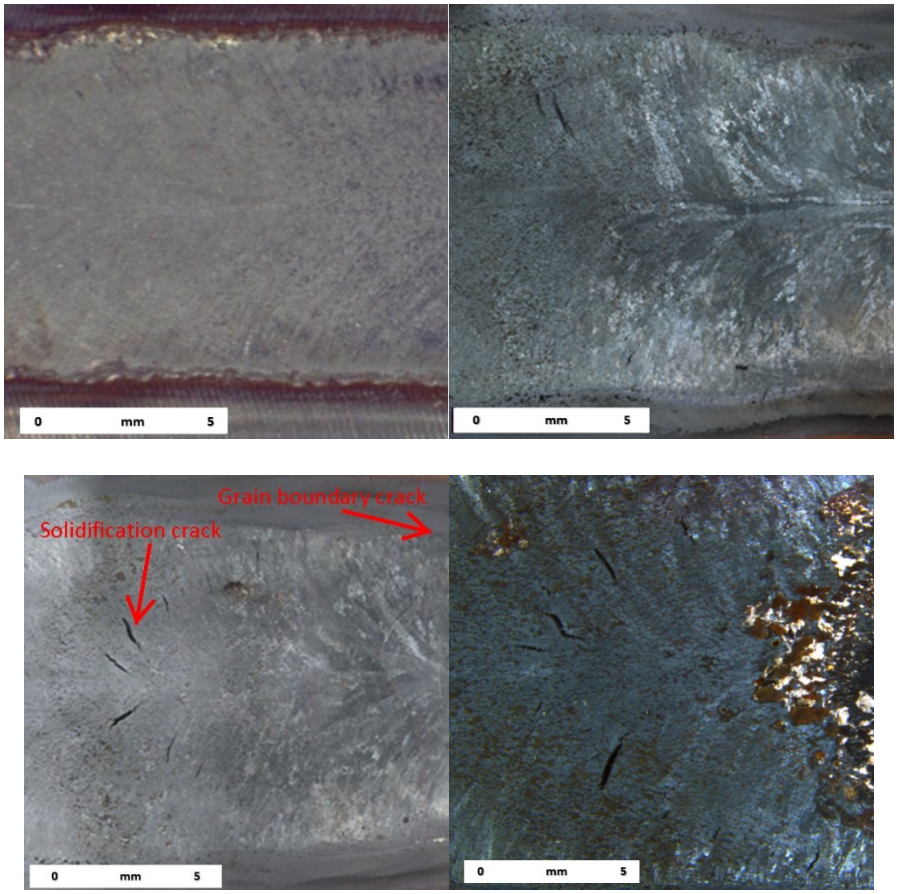


**Fig. 10**: Macrographs of welding surface of Varestraint specimens: D (top, left); E (top, right); F (bottom, left); G (bottom, right). D=20, E=35, F=44, G=50 ppm of boron respectively.

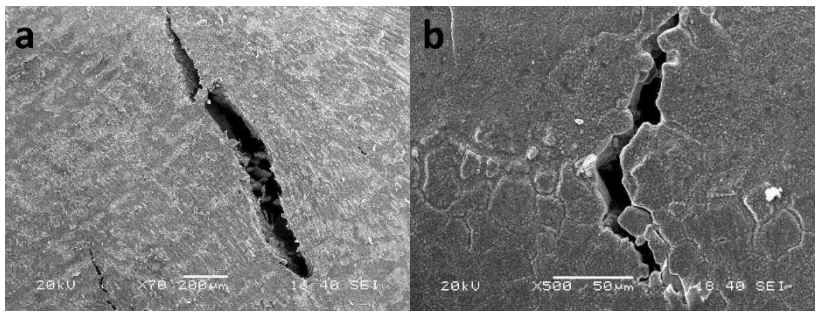


**Fig. 11**: SEM image of welding surface of F Varestraint specimen: a) solidification crack located close to the center of the fusion zone and b) grain boundary crack located near the fusion boundary.

Observation of specimen surface shows that the higher the boron content is, the more there are cracks. Even if grain boundary cracks are in the minority, high cracking sensibility of high boron content F and G stainless steels is confirmed. Few cracks appeared for E-specimen with 35 ppm of boron but with a deformation level of 7%, which is much higher than the real welding conditions for which strain level caused by thermal expansion is smaller than 2%.

*PVR tests*

PVR test consists of making a fusion line using bead-on-plate TIG-welding with argon shielding while the specimen is tensile loaded [19][20]. The welding torch moves with a constant speed while the strain rate increases from 0 to a maximal value with a constant acceleration (Figure 12). PVR tests were achieved on materials D, E, F and G.

The location of the first crack and those where the densities of cracks are 3 cracks/10mm and 9 cracks/10mm respectively were determined. Figure 13 shows the results obtained for each material.

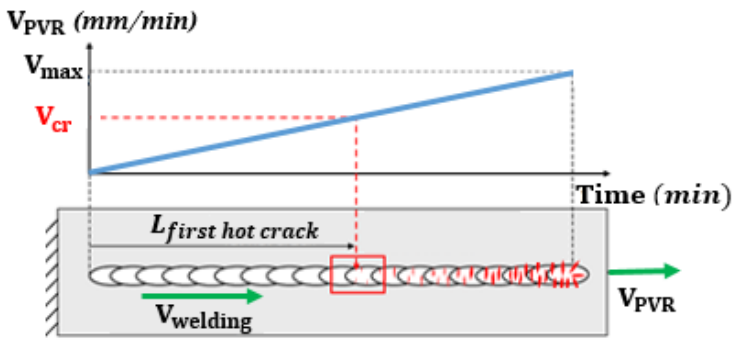


**Fig. 12**: Dependence of the ductility drop temperature with respect to boron content.

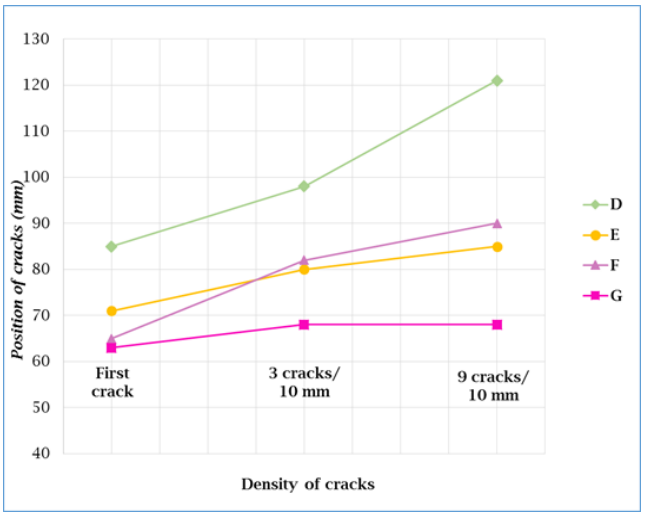


**Fig. 13**: Position of the first cracks for D, E, F and G materials in the PVR specimens. D=20, E=35, F=44, G=50 ppm of boron respectively.

The higher the boron content is, the earlier cracks appear. Therefore, the boron element has a negative effect on the cracking, even at a low content of 20 ppm (material D). However as for Varestraint tests, the direct surface observation did not allow to reveal grain boundary cracks. Thus a part of the welded surface of the F-specimen containing cracks was electrolytically etched to reveal the grain microstructure. Fig. 14 shows the results of this observation before and after the etching.

The cracks appear in the HAZ and are along grain boundaries, which is consistent with HAZ liquation cracking. As for Varestraint testing results', further analysis by transmission electron microscopy or X-ray microanalysis could be carried out to provide some evidence of liquated borides particles that would support this assumption. This experience was then repeated but at a depth of 0.5mm but no cracks were revealed (Fig. 15) highlighting the superficial character of cracking.

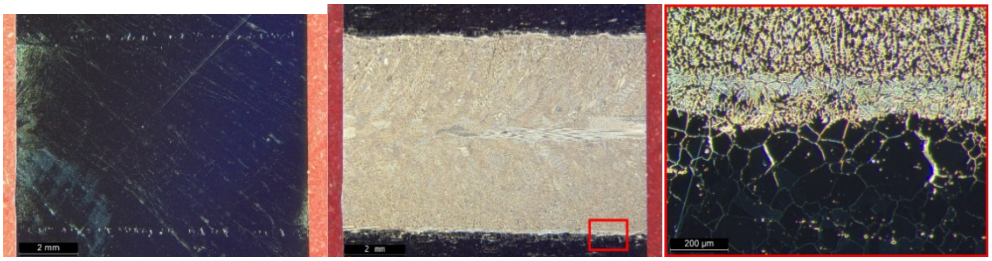


**Fig. 14**: Observation of a part of the welding surface of the PVR specimen F: before chemical attack (left) and after electrolytic etching (center and right).

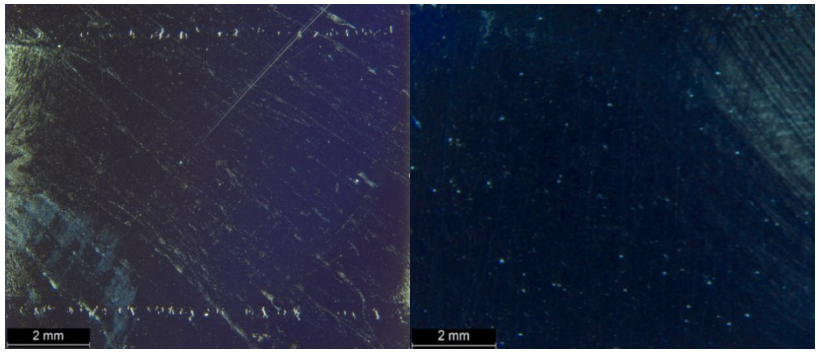


**Fig. 15**: Images at welding surface of PVR specimen F (left) and at depth of 0.5mm (right).

In the future, fracture surfaces could be obtained from Varestraint or PVR specimens in order to be compared to the fracture surfaces from the Gleeble tests.

## NUMERICAL MODELLING OF WELDABILITY

### GENERAL

Computational Welding Mechanics (CWM) provides access to physical quantities that are not accessible by other techniques for the purpose of understanding phenomena. These quantities can be treated qualitatively or quantitatively according to the objective and the level of modelling proposed. CWM generally relies on a three-dimensional model of the geometry discretized by finite elements to solve a thermal dependant problem thermal of solid mechanics. The thermal part of the analysis consists of solving the heat equation by modelling the energy input of the process with a mobile equivalent heat source. The parameters describing the spatial-temporal distribution of the heat source are based on the parameters of the welding process and they may be recalibrated with the help of experimental measurements. Thermo-mechanical coupling is achieved sequentially using the thermal history to solve the mechanical equilibrium at each time step while integrating the history effects according to an implicit scheme. An Elastic-Viscous-Plastic constitutive law (EVP) with mixed strain hardening is used to model the behaviour of the material between the ambient temperature and the solidus temperature. CWM was conducted with Code_Aster software [21] in accordance with the recommendations of CEN ISO / TS 18166: 2015 [22].

In order to access local thermomechanical conditions leading to hot cracking by liquation, the modelling effort focuses on the implementation of a detailed model dedicated to the simulation of PVR tests. In fact, the PVR tests are more discriminating than the Varestraint tests for treating the effect of boron on the weldability of the alloy.

*Heat transfers*

The heat input associated with the welding process is modeled by the equivalent heat source proposed by Goldak [23]. It is a double ellipsoid volumetric heat source whose intensity varies according to the position of the points with respect to the center of the source. This source moves at the speed of welding along the x axis. The function which describes the Goldak's source centered in ($x_0 = 0$, $y_0 = 0$, $z_0 = 0$) makes it possible to represent, in three dimensions, a source of heat with a Gaussian distribution of the power density. A generalized formula for the heat distribution is given in (1):

$$q_f(x,y,z) = Q_f \exp\left(-\frac{3(x-x_0)^2}{{a_f}^2} - \frac{(y-y_0)^2}{b^2} - \frac{(z-z_0)^2}{c^2}\right) pour\ x < x_0$$
$$q_r(x,y,z) = Q_r \exp\left(-\frac{3(x-x_0)^2}{{a_r}^2} - \frac{(y-y_0)^2}{b^2} - \frac{(z-z_0)^2}{c^2}\right) pour\ x < x_0 \quad (1)$$

In this case, it is assumed that the power transferred to the workpiece is given by ηUI with η the efficiency of the process, U the voltage and I the current of the generator. During TIG welding, the coupling between the arc and the weld pool leads to an asymmetry of the power distribution. This effect can be taken into account by considering parameter $Q_f$ and $a_f$ for the "front" of the source and parameters $Q_r$ and $a_r$ for the "back" of the heat source (2). To reduce the number of parameters to adjust we can add some relationships between $a_r$ and $a_f$ and $Q_r$ and $Q_f$. At each time step we must verify equation (2) over the workpiece domain Ω :

$$\iiint (q_f + q_r) d\Omega = \eta UI \quad (2)$$

Based on the size of the molten zone measured experimentally and on the response of thermocouples positioned on a PVR specimen, an iterative identification procedure made it possible to obtain the heat source parameters by successively replaying the thermal simulation, the results of which are shown in Fig. 16.

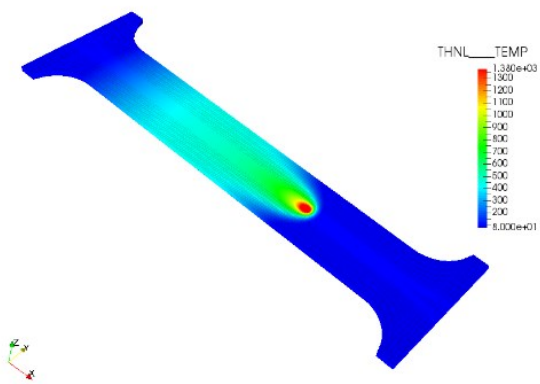


**Fig. 16**: Temperature field of the simulated PVR test at time 70 s.

*Mechanical analysis*

For the mechanical analysis, an elastoplastic law with mixed isotropic and kinematic hardening model and a Von Mises plasticity criteria have been used. Mechanical properties and thermal expansion varies with temperature. The phase transformation are not considered in the simulation as this material remains in a BCC crystal structure. Calculation is performed with small strains and displacements assumptions. The mixed isotropic–kinematic material hardening model was employed to produce the most representative material response to the cyclic thermo-mechanical loading imposed during welding. The model used is derived from Lemaitre-Chaboche model [24] with a tensor of kinematic non-linear hardening taking into account Bauschinger effect and cyclic hardening with plastic shakedown, a nonlinear isotropic hardening. Viscous effect are also considered. All the properties of material depend on the temperature. The model is called VISC_CIN1_CHAB in CODE_ASTER [21]. The isotropic hardening component which defines the evolution of the yield surface, R(p), where p is the cumulative plastic strain, is defined as follows (3):

$$R(p) = R_I + (R_0 - R_I)e^{-bp} \tag{3}$$

Where $R_0$ and $R_t$ are the yield stress at zero plastic strain, and the maximum yield surface size respectively. b defines the rate at which the size of the yield surface changes as plastic strain develops. The kinematic hardening component is defined as a combination of a kinematic term and a relaxation term. The kinematic hardening law is defined as follows (4):

$$\begin{aligned} \underline{\underline{X}} &= \tfrac{2}{3} C(p)\underline{\underline{\alpha}} \\ \dot{\underline{\underline{\alpha}}} &= \dot{\underline{\underline{\epsilon}}}_p - G(p)\dot{\underline{\underline{\epsilon}}}_p p \end{aligned} \tag{4}$$

Where C(p) and G(p) are material parameters that can depend on the cumulative plastic strain, $\underline{\underline{\alpha}}$ is the back-stress tensor, $\dot{\underline{\underline{\epsilon}}}_p$ is the equivalent plastic strain rate.

A Norton law is used to consider viscous effects (5):

$$\dot{p} = \left(\frac{\langle F \rangle}{K}\right)^N \quad \text{with} \quad F\left(\underline{\underline{\sigma}}, R, \underline{\underline{X}}\right) = \sqrt{\tfrac{3}{2}\left(\underline{\underline{\overline{\sigma}}} - \underline{\underline{X}}\right) : \left(\underline{\underline{\overline{\sigma}}} - \underline{\underline{X}}\right)} - R(p) \tag{5}$$

Where <F> is the positive part of F and $\underline{\underline{\overline{\sigma}}}$ the deviatoric part of the stress tensor. K, N as well as parameters C(p), G(p) and b depend on the temperature. Table 3 gives the mechanical properties of the material proposed by LE [25] and adjusted to fit the load – displacement curve measured during the PVR test (see Fig. 17). The first crack appears for a displacement of 1.5 mm (material G, red region), and with material D (green region), the first crack appears for a displacement of 2.7 mm.

**Table 3** Elastic, Plastic and Viscous properties.

| | E [MPa] | $R_0$ [MPa] | $R_I$ [MPa] | b | K [MPa] | N | C [MPa] | G |
|---|---|---|---|---|---|---|---|---|
| **20°C** | 190000 | 60 | 120 | 8 | 151 | 24 | 30000 | 350 |
| **600°C** | 140000 | 10 | 80 | 8 | 150 | 12 | 24810 | 300 |

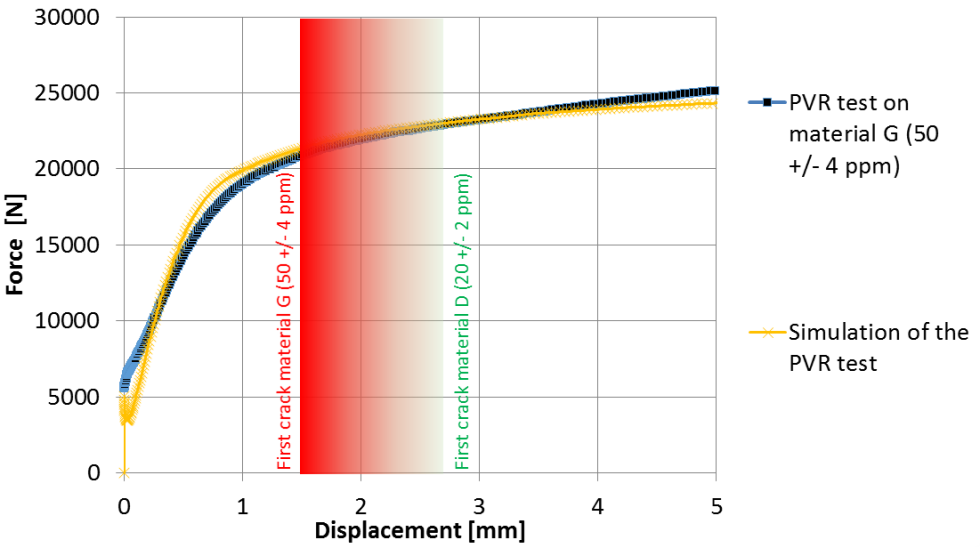


**Fig. 17**: Load-displacement curve for PVR test performed with material G. Comparison between measurements and simulation.

## CRITERIA FOR THE ASSESSMENT OF HOT CRACKING RISK

Let us consider the two following experimental results: the sensitivity to the hot cracking by liquation determined by the hot ductility tests and the position of the first crack of the PVR test as a function of the boron content. The sensitivity to hot cracking by liquation is described by the surface response (see Fig. 18) derived from the hot ductility tests in a 3-dimensionnal space: boron content, ductility drop temperature and holding time.

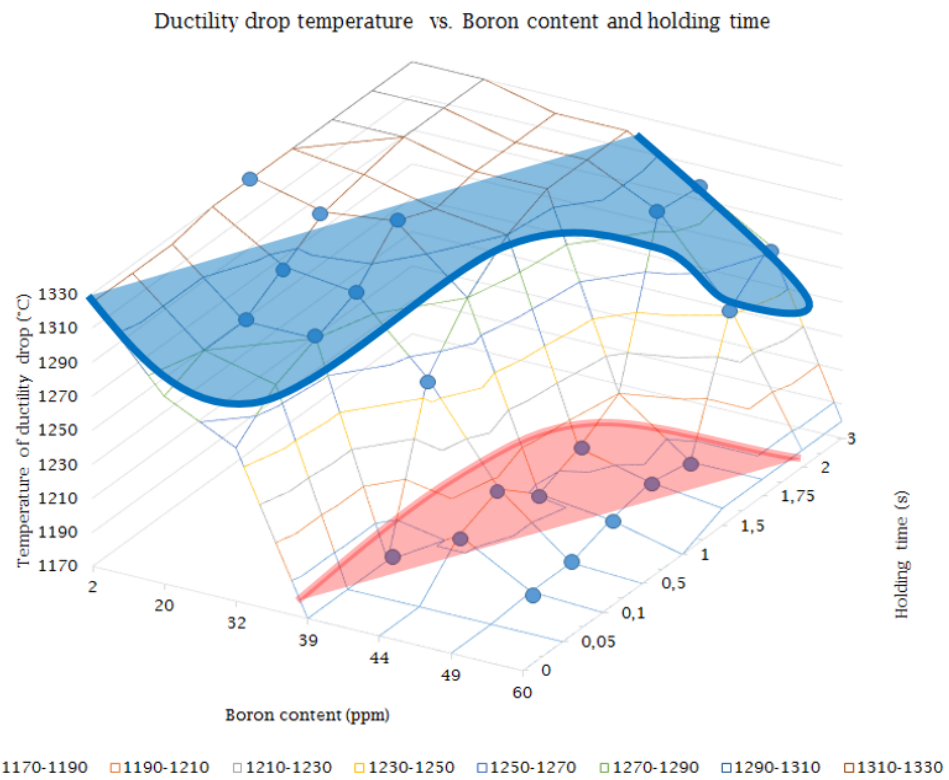


**Fig. 18**: Surface response derived from the hot ductility tests: ductility drop temperature as a function of boron content and holding time.

Fig. 18 shows a transition in the evolution of material sensitivity versus boron content between 39 and 44 ppm. In fact, for boron contents below 39 ppm, the ductility drop temperature remains high and tends to increase with the holding time. Conversely, for boron contents above 39 ppm, the ductility drop temperature is low for holding times of less than 2 s. This temperature increases significantly for holding times greater than 2 s to reach values however lower than for alloys with low boron content. Fig. 13 shows the position of the first crack as well as the position for which the crack densities are 3 cracks / 10 mm and 9 cracks / 10 mm, depending on the boron content (cracks detected by liquid penetrant testing). These results make it possible to define the position of the first crack as a function of the boron content to be considered conservatively for the establishment of the criteria. For the boron content of 20 ppm, the first crack appears late at a distance of 85 mm. For the boron content of 35 ppm, the distance is 71 mm, for the highest contents, the distance is between 60 and 65 mm. The positions at 60 and 85 mm constitute the boundaries of an area in which the cracking conditions are met (boron content, holding time and ductility drop temperature). The fact that the PVR test is an external mechanical stress test allows to integrate an additional parameter which involves the level of stress applied to the zone of ductility drop. This level of stress is determined by the numerical simulation of the test. A tensile stress seems to be a sufficient condition to create liquation cracks because they make it possible to overcome the cohesive strength between two grain boundaries and the liquid

film. In the case of the PVR test, it is a uniaxial tension (in the tensile x direction of welding) and the cracks observed are perpendicular to this direction. Therefore, only the constraint component in this direction, $\sigma_{xx}$, is considered. This approach can be generalized in a real welding case considering the maximum principle stress. The simplest way to integrate this quantity into the criteria is to compare it with a threshold value. If the local value of the stress is greater than the threshold value, there is a risk of hot cracking. To determine this threshold stress, it is possible to post-process stress-temperature-time curves from the simulation results at different points in the HAZ of the model. The 3-dimensional stress-temperature-time curves extracted at different points in the specimen can be used for comparison with the experimental ductility drop characterizations. The points studied correspond to the position where the first cracks appear for each boron content (see Fig. 19).

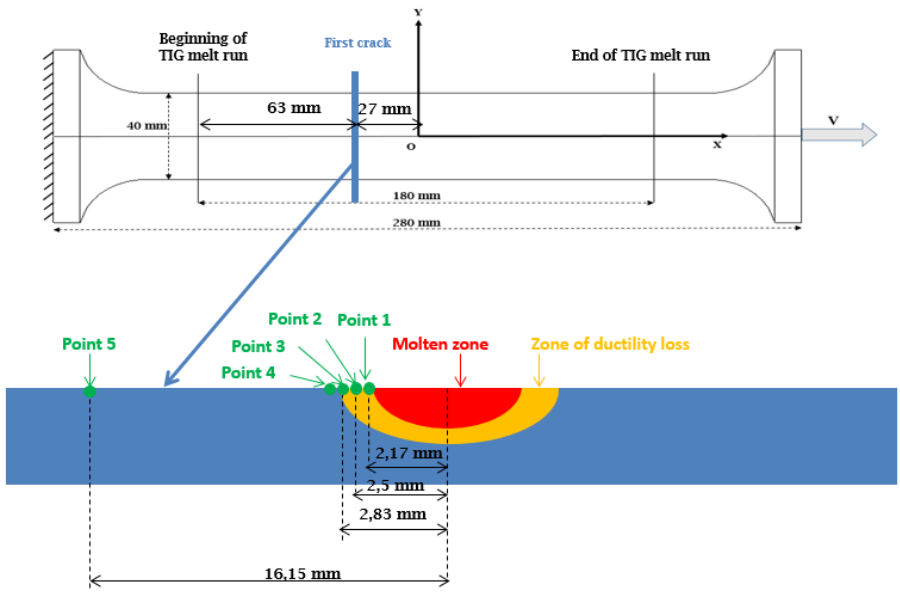


**Fig. 19**: Position along the specimen and through the section where stress-temperature-time curves are post-processed to determine stress threshold.

To facilitate the analysis, these curves are plotted in a two-dimensional stress - temperature space. Time is represented by markers on the curve. Fig. 20 shows an example for two points in the HAZ at the two positions 40 mm and 80 mm along the specimen, four points in total. The time between two markers is 0.25 s. It is possible to plot the evolution of the stress in the temperature range presenting a risk of ductility loss by liquation with a maximum temperature of the order of 1400°C for the point 1 close to the molten zone and 1200°C for point 3.

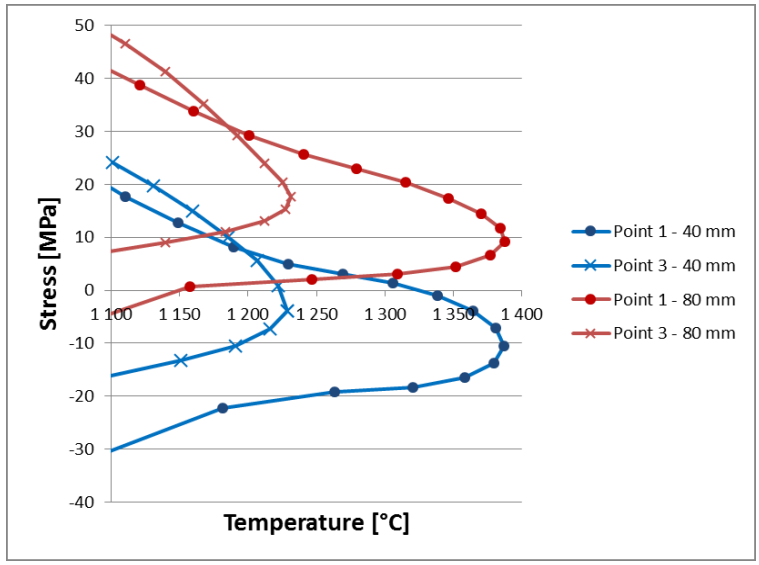


**Fig. 20**: Stress versus temperature curves at different locations along the specimen (40 and 80 mm from the fusion line start) and two positions in the HAZ (point 1 close to the molten zone and 3).

To determine a stress threshold below which the risk of hot cracking by liquation is null whatever the temperature, the holding time and the boron content are, it is necessary to base the analysis, in a conservative manner, on the test which shows a crack for the lowest stress. This is the PVR test conducted on the most sensitive to hot cracking material which contains 50 ppm of boron (material G). The ductility drop temperature measured for this boron content is of the order of 1180°C and the holding time necessary to recover its ductility is greater than 2 s. The position of the first crack for this test is 63 mm from the start of the melting line. Fig. 21 shows the evolution of the stress as a function of temperature at this position for several points in the HAZ. The threshold stress corresponds to the stress reached before the material recovers its ductility, after 2 s spent above the lowest ductility drop temperature. Conservatively, the lowest threshold stress level is obtained from the stress-temperature curve of the nearest point of the melted zone. The holding time above 1180 ° C is greater than 2 s (contains more than 8 intervals of 0.25 s) when the cooling stress reaches 10 MPa. The threshold stress value below which the risk of hot cracking by liquation is excluded is set at 10 MPa.

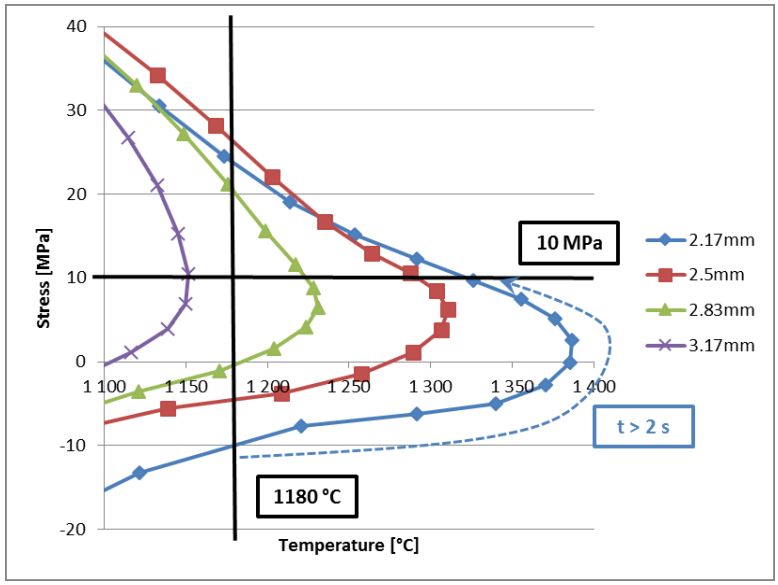


**Fig. 21**: Stress versus temperature curve at the 63 mm position of the first crack for the highest boron content (material G) for different points in the HAZ.

Fig. 22 allows to follow the evolution of the stress as a function of the temperature at the position of the first crack for the material least susceptible to cracking at different points of the HAZ, close to the molten zone. Holding times are relatively low to recover the ductility of the material for this boron content (material D containing 20 ppm boron). These holding times of order of 0.5 s are possible for points whose maximum reached temperature is close to the ductility drop temperature defined at 1280°C (point of the red curve in Fig. 22). This analysis makes it possible to confirm the presence of a point exceeding the threshold stress before its ductility is recovered and thus the presence of a crack at 85 mm for this material.

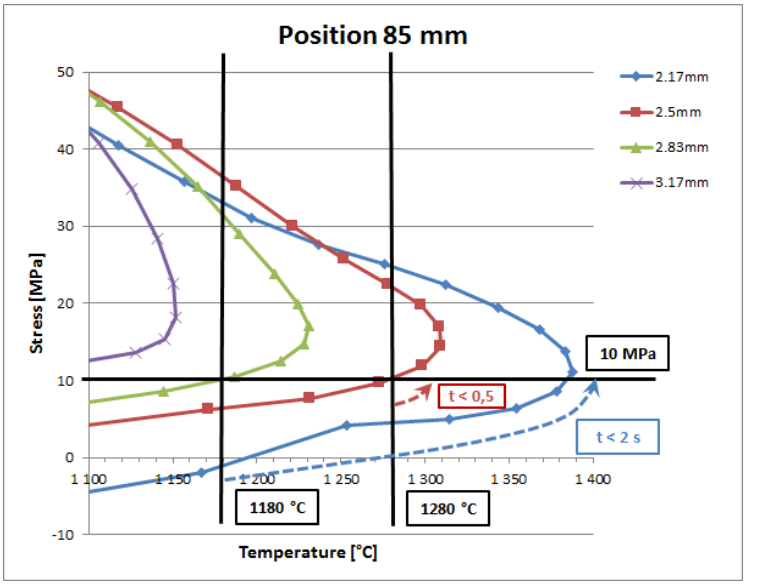


**Fig. 22**: Stress versus temperature curve at the 85 mm position of the first crack for the lowest boron content (material D): point 1 very close to the melted zone (blue curve), and point 2 which reaches the threshold stress for a low holding time low (<0.5 s).

Fig. 23 allows to follow the evolution of the stress as a function of the temperature at the position of the first crack for the material E (35 ppm of boron content) which marks a transition with respect to the sensitivity to the loss of ductility (see Fig. 1, Fig. 2 and Fig. 18). The holding times are relatively low to recover the ductility for the material E. These holding times, of the order of 0.5 s, are possible for points whose maximum reached temperature is close to the temperature of ductility drop defined at 1280°C (red curve in Fig. 23). This analysis makes it possible to confirm the presence of a point exceeding the threshold stress before its ductility is recovered and thus the presence of a crack at 71 mm. For slightly higher boron content and a material whose ductility drop temperature approaching 1180°C, the holding time remains less than 2 s, which is consistent with the presence of liquation cracks observed in this area for material F.

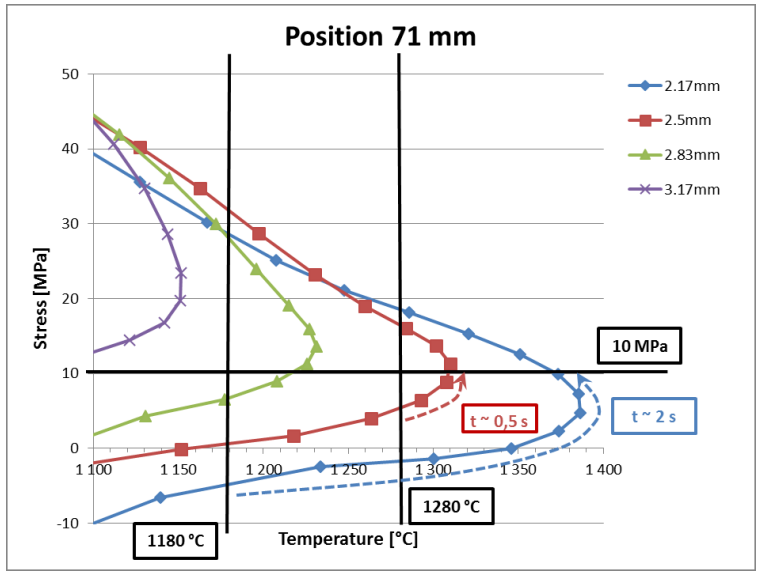


**Fig. 23**: Stress versus temperature curves at the 71 mm position of the first crack for the 35 ppm grade (material E).

On the basis of these analyzes, the criteria for the assessment of liquation hot cracking risk for 316L austenitic stainless steel can be stated as follows: at positions where the maximum temperature reached is between 1150°C and 1350°C, only points with a maximum stress above10 MPa during cooling present a risk of cracking:

- For materials with a boron content lower than 35 ppm, the risk becomes null if the holding time above 1280°C is greater than 0.5 s.
- For materials with a boron content greater than 35 ppm, the risk becomes null if the holding time above 1180°C is greater than 2 s.

## CONCLUSION

- The ductility drop temperature transition in type 316L steel occurs for a boron content between 35 ppm and 44 ppm. This is in agreement with the results of literature.
- The holding time at on-heating testing temperature increases the ductility drop temperature, so decreases the risk of HAZ liquation cracking. SIMS analysis are consistent with the hypothesis of boron diffusion from grain boundaries towards the austenitic matrix. Even a short holding times would be sufficient to prevent grain boundary melting.
- An equivalent time defined as the duration time over the testing temperature on heating in addition is considered to conduct on cooling test. A coherence between the on-cooling and on-heating results is found. For the low temperature test achieved under 1260°C, the duration time is long and there is no risk of cracking. For the high temperature tests, the duration time becomes shorter, ductility falls down and the risk of cracking increases.

- The Varestraint and PVR tests show that boron does have a negative impact on the hot cracking suceptibility: the higher the boron content, the more susceptible to hot cracking the steel is. Near the fusion zone boundary cracking along grain boundaries is visible on SEM images which is coherent with liquation cracking phenomenon.
- The experimental program has thus demonstrated that the 316L type of austenitic stainless steel studied does not exhibit weldability issues such as liquation hot cracking under the effect of the boron content if the boron content remains less than 35 ppm.
- The PVR test results are consistent with ductility test, they highlight the effect of boron content on the grain boundary crack susceptibility. The results of the PVR test and its simulation are used to determine a criteria for HAZ liquation cracking, taking into account of the boron content and the stress level.
- The proposed criteria states that for material with a boron content greater than 35 ppm, the risk is canceled if the holding time above 1180°C is greater than 2 s.
- The type 316L austenitic stainless steel do not highlight weldability issues such as boron assisted liquation cracking if the boron content remains below 35 ppm. In addition, real welding tests could be carried out to confirm this point. The degree of conservatism of the proposed criterion could thus be evaluated by simulation of these configuration, which would make it possible to release margins according to the welding configurations in order, for example, to relax the specification on the boron content in procurement procedures while securing the fabrications by increasing the holding times in the [1150°C – 1350°C] temperature range (preheating, welding energy ...).

## REFERENCES


[1] E. FOLKHARD: *Welding metallurgy of stainless steels,* Springer-Verlag Wien, New York, 1988.

[2] JC. LIPPOLD: *Welding metallurgy and weldability*, John Wiley & Sons, Inc, 2014.

[3] R.D. THOMAS JR.: 'HAZ cracking in thick sections of austenitic stainless steels - Part II', *Welding Journal*, 63(9), pp. 355s-368s, 1984.

[4] X. HUANG, M. C. CHATURVEDI, N. L. RICHARDS AND J. JACKMAN: 'The effect of grain boundary segregation of boron in cast alloy 718 on HAZ microfissuring - a SIMS analysis', *Acta materiala*, 45 (8), pp. 3095-3107, 1997.

[5] R.K. SIDHU, O.A. OJO AND M.C. CHATURVEDI: 'Microstructural response of directionally solidified René 80 superalloy to gas-tungsten arc welding', *Metallurgical and Materials Transactions*, 40A, pp. 150-162, 2009.

[6] H. GUO, M.C. CHATURVEDI & N.L. RICHARDS: 'Effect of boron concentration and grain size on weld heat affected zone microfissuring in Inconel 718 base superalloys', *Science and Technology of Welding and Joining*, 4(4), pp. 257-264, 2013.

[7] W. CHEN, M.C CHATUVERDI AND N.L. RICHARDS: 'Effect of boron segregation at grain boundaries on heat-affected zone cracking in wrought Inconel 718', *Met. and Mat. Trans. A*, 32A, pp. 931-939, 2001.

[8] O.A. OJO AND M.C. CHATUVERDI: 'Liquation microfissuring in the weld heat-affected zone of an overaged precipitation-hardened nickel-base superalloy', *Metallurgical and Materials Transactions*, 38A, pp. 356-369, 2007.

[9] G. LI, X. LU, X. ZHU, J. HUANG, L. LIU AND Y. WU: 'The Segregation and Liquation Crackings in the HAZ of Multipass Laser-Welded Joints for Nuclear Power Plants', *Journal of Materials Engineering and Performance*, 26(8), 4083-4091, 2007.
[10] G. ZACHARIE: 'Influence du bore sur la résistance à la fissuration à chaud dans les zones affectées par le soudage et sur la tenue au fluage des aciers 18-10Ti', *PhD dissertation*, Université de Paris-Sud, 1978.
[11] J.R. DONATI, D. GUTTMANN AND G. ZACHARIE: 'Influence de la teneur en bore sur la fissuration à chaud d'aciers 18-10', *Revue de Metallurgie (Paris)*, 71(12), pp. 917-930, 1974.
[12] ISO/TR 17641-3: 'Destructive Tests On Welds In Metallic Materials - Hot Cracking Tests For Weldments - Arc Welding Processes', 2005.
[13] G. SRINIVASAN, M. DIVYA, C. R. DAS, S. K. ALBERT, A. K. BHADURRI, S. LAUF, S.TUBENRAUCH, A. KLENK (2015): 'Weldability studies on borated stainless steel using Varestraint and Gleeble tests', *Welding World*, 59, pp. 119-126, 2015.
[14] W. LIN, J.C. LIPPOLD AND W.A. BAESLACK: 'An evaluation of heat affected zone liquation cracking susceptibility Part I', *Welding Journal*, 71(4), pp. 135s–153s, 1993.
[15] R. BOUDOT AND G. ZACHARIE: 'Influence de la teneur en bore sur la résistance à la fissuration à chaud dans les zones affectées par le soudage d'acier 18%Cr-12%Ni au molybdène en relation avec le mode d'élaboration', *25ème Colloque de Métallurgie - Progrès Récents dans l'Elaboration des Métaux et Alliage, Conséquences sur leur Propriétés d'Emploi*, Saclay, 23-25 Juin 1982.
[16] L. KARLSSON, H. NORDÉN AND H. ODELIUS: 'Non-equilibrium grain boundary segregation of boron in austenitic stainless steel - I. Large scale segregation behavior', *Acta metallurgica*, 36 (1), pp. 1-12, 1988.
[17] L.O. OSOBA, Z. GAO AND O.A. OJO: 'Physical and numerical simulations study of heat input dependence of HAZ cracking in nickel base superalloy IN 718', *Journal of Metallurgical Engineering* (ME), 2 (3), pp. 88-93, 2013.
[18] C. D. LUNDIN ET AL. : 'Hot ductility and hot cracking behaviour of Modified 316 Stainless Steels designed for high temperature service', *Welding Journal* , 72(5), pp. 189s-200s, 1993.
[19] T. KANNENGIESSER, K. BOELLINGHAUS : 'Hot cracking test. An overview of present technologies and applications', *Welding World*, 58(3), pp. 397-421, 2014.
[20] G. TIRAND, C. PRIMAULT, V. ROBIN: 'Sensibilité à la fissuration à chaud des alliages base nickel à haute teneur en chrome, High chromium nickel base alloys hot cracking susceptibility', *Matériaux & Techniques*, 102(4), 403, pp. 1-5, 2014.
[21] CODE_ASTER, version 13.4, https://www.code-aster.org/, 2017
[22] CEN ISO/TS 18166:2015, 'Numerical welding simulation — Execution and documentation', 2015.
[23] J.A. GOLDAK, A. CHAKRAVARTI, J. BIBBY: 'A new finite element model for welding heat sources', *Metallurgical Transactions*, 15B, pp. 299-305, 1984.
[24] J. LEMAITRE, J.L. CHABOCHE: 'Mechanics of Solid Materials', *Cambridge University Press*, 1990.
[25] M. LE, 'Approches expérimentale et numérique de la fissuration à chaud dans les soudures en acier inoxydable, *PhD Thesis*, Université de Bretagne Sud, France, 2014.